UK Atomic Energy Authority

UKAEA-STEP-PR(23)10

M. Giacomin, D. Kennedy, C. J. Ajay, D. Dickinson, B. S. Patel, C. M. Roach

Electromagnetic gyrokinetic instabilities in the Spherical Tokamak for Energy Production (STEP) part II: transport and turbulence

Electromagnetic gyrokinetic instabilities in the Spherical Tokamak for Energy Production (STEP) part II: transport and turbulence

M. Giacomin, D. Kennedy, C. J. Ajay, D. Dickinson, B. S. Patel, C. M. Roach

This is a preprint of a paper submitted for publication in Nuclear Fusion

Electromagnetic gyrokinetic instabilities in the Spherical Tokamak for Energy Production (STEP) part II: transport and turbulence

M. Giacomin[1], D. Kennedy[2], F. J. Casson[2], Ajay C. J.[3], D. Dickinson[1], B. S. Patel[2] and C. M. Roach[2]

[1]York Plasma Institute, University of York, York, YO10 5DD, United Kingdom
[2]Culham Centre for Fusion Energy, Abingdon, OX14 3DB, United Kingdom
[3]Centre for Fusion, Space and Astrophysics, Department of Physics, University of Warwick, Coventry, CV4 7AL, United Kingdom

E-mail: maurizio.giacomin@york.ac.uk

Abstract.

In this work, we present the results of first-of-their-kind nonlinear local gyrokinetic simulations of electromagnetic turbulence at mid-radius in the burning plasma phase of the conceptual high-β, reactor-scale, tight-aspect-ratio tokamak STEP (Spherical Tokamak for Energy Production). A prior linear analysis in D.Kennedy *et al.* submitted to Nucl. Fusion [1] reveals the presence of unstable hybrid kinetic ballooning modes and subdominant microtearing modes at binormal scales approaching the ion-Larmor radius. Local nonlinear gyrokinetic simulations, using three different codes, are in qualitative and quantitative agreement and suggest that hybrid kinetic ballooning modes drive very large turbulent transport in the absence of equilibrium flow shear. The heat flux rises to values that exceed the available heating power by orders of magnitude and the turbulent eddies are highly extended radially so that they may not be well described by the local gyrokinetic model. The saturated transport fluxes are extremely sensitive to equilibrium flow shear, and diamagnetic levels of flow shear can suppress the fluxes to more reasonable values on the chosen surface. Given this sensitivity there is a large uncertainty in the saturated fluxes. The possible transport impact of the subdominant microtearing modes is also analysed in isolation by artificially and unphysically removing compressional magnetic perturbations from nonlinear calculations, to suppress the dominant hybrid kinetic ballooning mode. The microtearing heat flux is found to saturate at negligible values, though we cannot exclude the possibility that microtearing turbulence may be more transport relevant in other regions of parameter space.

1. Introduction

Understanding and predicting turbulence in the core of next-generation spherical tokamaks (STs) is critical for the optimisation of their performance. While there has been progress over the past two decades, previous attempts to predict turbulent transport from local nonlinear electromagnetic gyrokinetic (GK) simulations for

conceptual ST power plant equilibria have found large runaway transport fluxes dominated by magnetic flutter at low wavenumber, with heat fluxes orders of magnitude greater than the available heating power [2, 3].

By leveraging the properties of STs, the UK STEP programme aims to generate net electric power $P_{\mathrm{el}} > 100$ MW from fusion [4, 5], by developing a compact prototype power plant based on the ST. The first phase of this ambitious programme is to provide a conceptual design of a STEP prototype plant and a reference equilibrium for the preferred flat-top operating point.

In order to be economically competitive, ST power plants such as STEP require a high ratio of thermal pressure to magnetic pressure, β, in the tokamak core. At high β the turbulence is expected to become more electromagnetic in nature, and influenced by unstable kinetic ballooning modes (KBMs) and microtearing modes (MTMs), as frequently reported for STs (see [6] and references therein). Whilst GK simulations have thus far proven to be a reliable tool for modelling turbulent transport in predominantly electrostatic regimes in conventional aspect ratio tokamaks at low β, obtaining saturated nonlinear simulations of plasmas at higher β with unstable KBMs and MTMs is computationally and conceptually more challenging. A runaway transition to very large heat flux can occur in local nonlinear simulations even at β values that are smaller than the critical threshold for the onset of the KBM instability, when the dominant instability is an ion temperature gradient (ITG) or a trapped electron mode (TEM) [7]. It remains an open question as to whether these runaway transitions are robustly physical, or a result of important physics being missing in the local GK model.

Various plasma reference scenarios for STEP have been developed by using the integrated modelling suite JINTRAC [8] using the JETTO transport module, and assuming a Bohm-gyro-Bohm model [9] that has been recalibrated to have dominant electron heat transport and $H_{98} = 1.3$ in STEP conditions [10,11]. Given the likely more significant role of electromagnetic instabilities in the core of high-β STs with respect to conventional tokamaks, the transport and confinement assumptions used to develop the STEP scenarios need to be assessed by means of first-principles GK simulations, which motivates the present work. Among the different plasma reference scenarios, we focus here on STEP-EC-HD-v5 ‡(hereinafter STEP-EC-HD), designed to deliver a fusion power $P_{\mathrm{fus}} = 1.8$ GW. The global parameters for this plasma scenario are reported in [1]. A contour plot of the poloidal magnetic flux Ψ in STEP-EC-HD is shown in Figure 1, alongside radial profiles of the three plasma species (electron, deuterium and tritium) included in the following gyrokinetic analysis, which is carried out at the $q = 3.5$ surface (where the normalised poloidal flux is $\Psi_n = 0.49$), which is highlighted in red in Figure 1.

A Miller parameterisation [12] was used to model the local plasma equilibrium, and the shaping parameters were fitted to the chosen surface using `pyrokinetics` [13], a python library developed to facilitate pre- and post-processing of gyrokinetic analysis using a range of different GK codes. `Pyrokinetics` was also used throughout to facilitate

‡ SimDB UUID: 2bb77572-d832-11ec-b2e3-679f5f37cafe, Alias: smars/jetto/step/88888/apr2922/seq-1

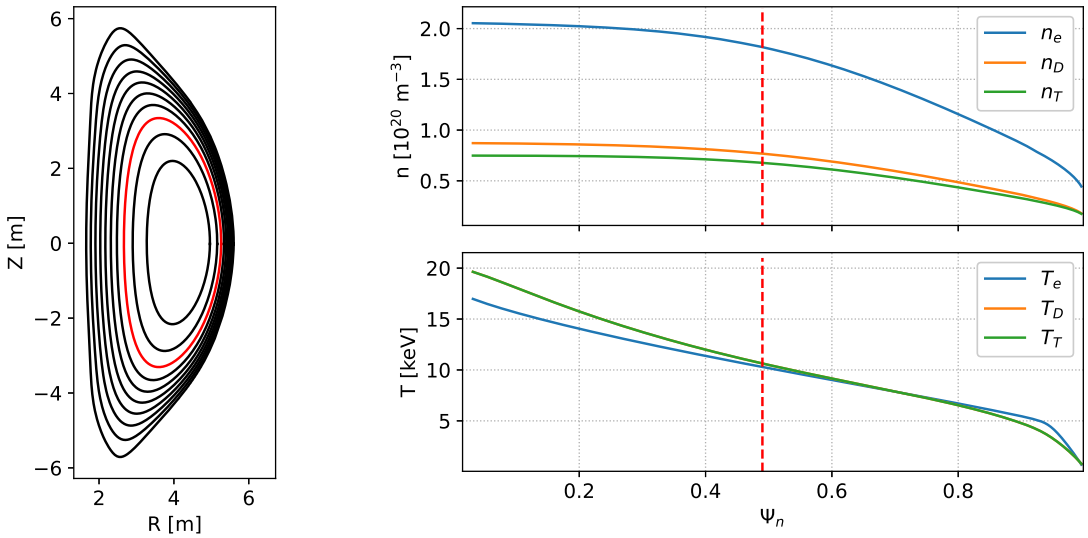

(a) **(b)**

Figure 1: *(a) Contour plot of the poloidal magnetic flux in the STEP-EC-HD equilibrium. The red line denotes the flux surface corresponding to $q = 3.5$. (b) Density and temperature profiles of electrons, deuterium and tritium (the three species considered in the present analysis) as functions of the normalised poloidal flux, Ψ_n, from the STEP-EC-HD equilibrium. Impurities and helium species are neglected.*

the conversion of input files between the different local GK codes used in this work. Table 1 provides the values of various local equilibrium quantities at the $q = 3.5$ ($\Psi_n = 0.49$) surface: magnetic shear, $\hat{s}$; normalised minor radius, ρ/a; elongation and its radial derivative, κ and κ'; triangularity and its radial derivative, δ and δ'; radial derivative of the Shafranov shift, Δ'; temperature T and density n for electrons, deuterium and tritium, and their normalised inverse gradient scale lengths. Whilst this analysis is restricted to $\Psi_n = 0.49$, we expect results and conclusions to be relevant across a range of surfaces that share qualitatively similar linear microstability properties in this STEP reference plasma [1].

The local linear GK analysis of the $q = 3.5$ surface ($\Psi_n = 0.49$) in STEP-EC-HD is reported in a companion article [1]. This analysis (see in particular Figures 19 and 20 of [1]) shows the presence of a dominant ion Larmor radius scale hybrid KBM instability that couples to a trapped electron mode (TEM) and to an ion temperature gradient (ITG) instability at low β. A subdominant MTM was found to be unstable on a subset of these binormal scales. No unstable microinstabilities are observed at the electron Larmor radius scale. The linear growth rate and mode frequency are shown in Figure 2 as functions of the binormal wave-number $k_y\rho_s = n\rho_* \mathrm{d}\rho/\mathrm{d}\Psi_n$ (where n is the toroidal mode number, $\rho = r/a$ is the normalised minor radius, $\rho_* = \rho_s/a$, with $\rho_s = c_s/\Omega_D$ the deuterium Larmor radius, $c_s = \sqrt{T_e/m_D}$ the deuterium sound speed,

Parameter	**Value**	**Parameter**	**Value**
Ψ_n	0.49	B_0 [T]	2.8
q	3.5	n_e [10^{20}m^{-3}]	1.81
$\hat{s}$	1.2	T_e [keV]	10.3
κ	2.56	ρ_s [mm]	5.2
κ'	0.06	n_D/n_e	0.53
δ	0.29	n_T/n_e	0.47
δ'	0.46	T_D/T_e	1.03
Δ'	-0.40	T_T/T_e	1.03
β_e	0.09	a/L_{n_e}	1.03
β'	-0.48	a/L_{n_D}	1.06
r [m]	1.3	a/L_{n_T}	0.99
R [m]	4.0	a/L_{T_e}	1.58
A_{surf} [m^2]	370	a/L_{T_D}	1.82
P_{surf} [MW]	500	a/L_{T_T}	1.82

Table 1: *Local parameters at the $q = 3.5$ surface of the STEP-EC-HD equilibrium considered in the local gyrokinetic nonlinear analysis. Parameters not defined in the text include: electron plasma $\beta_e = 2\mu_0 n_e T_e/B_0$; radial derivative of a quantity X, denoted as $X' = \frac{dX}{d\rho}$; minor and major radii, r and R; surface area A_{surf}; power crossing the surface P_{surf}; density n_s and temperature T_s for species s; and normalised inverse gradient scale lengths defined for X as $a/L_X = \frac{a}{X}\frac{\mathrm{d}X}{\mathrm{d}\rho}$, with a the minor radius of the last-closed flux surface.*

$\Omega_D = eB_0/m_D$ the deuterium cyclotron frequency, and B_0 the vacuum toroidal magnetic field at the centre of the chosen flux surface). Reference [1] also points out the critical role played by compressional magnetic fluctuations ($\delta B_\parallel$). If $\delta B_\parallel$ is artificially excluded from calculations, the hybrid KBM is entirely stabilised while the linear properties of the MTM are unaffected. Here we model the turbulent transport that might be expected to be driven by these two classes of mode.

The main contributions of this work are: (a) to provide a detailed study of turbulent transport using local nonlinear gyrokinetic simulations in the core region of a STEP flat-top operating point; (b) to assess the compatibility of the predicted transport with the anticipated sources in STEP; (c) to explore different strategies for reducing transport in the conceptual STEP design; (d) to compare results using three local GK codes (simulations are performed using CGYRO [14] (commit `399deb4c`), GENE [15] (commit `de99981`), and GS2 [16] (commit `675f0870`)) in order to build confidence in transport predictions in this novel regime.

In all the simulations, we retain three particle species (electrons, deuterium and tritium) as well as electromagnetic effects. Simulations are performed to separately study the hybrid KBM-driven turbulence (by retaining both perpendicular and parallel

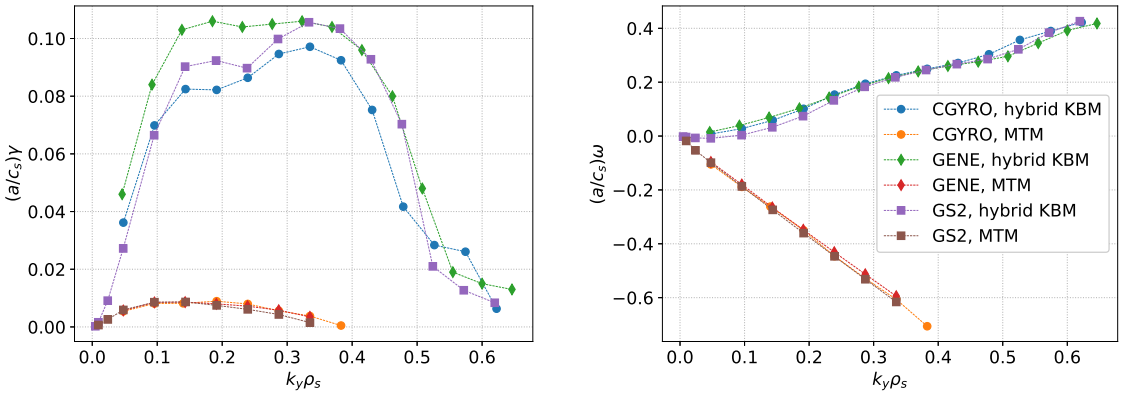

(a) **(b)**

Figure 2: *Growth rate (a) and mode frequency (b) as a function of $k_y\rho_s$ from CGYRO, GENE and GS2 linear simulations of the dominant (hybrid KBM) and subdominant (MTM) instabilities of STEP-EC-HD at the radial surface corresponding to $q = 3.5$ (adapted from Figures 19 and 20 of Reference [1]).*

magnetic field fluctuations) and MTM-driven turbulence (where hybrid KBMs are artificially suppressed through the neglect of $\delta B_\parallel$). In all cases we use full expressions for the ∇B and curvature drifts without approximation (i.e. we retain the ∇p contribution to the curvature drift). Collisions are modelled using the advanced Sugama collision model [17] in CGYRO and GENE, and the linearised Fokker-Planck collision model of [18] in GS2.

The paper is organised as follows. In §2, we present the results of nonlinear local (flux-tube) gyrokinetic simulations including $\delta B_\parallel$ carried out with CGYRO, GENE and GS2, and we discuss the sensitivity to the numerical parameters. The effect of equilibrium flow shear is investigated in §3. In §4, we evaluate the sensitivity of the heat flux to several key local equilibrium parameters. The results of nonlinear simulations where $\delta B_\parallel$ is artificially suppressed and the turbulence is driven solely by MTMs are shown in §5. Finally, a summary of our findings is presented in §6.

2. Nonlinear simulations including $\delta B_\parallel$ and cross-code comparison

We analyse here the results of nonlinear gyrokinetic simulations of the main hybrid KBM instability. As reported in [1], this instability is dominant at binormal scales approaching the ion Larmor scale across a range of different flux surfaces between the core and the pedestal top. These simulations are fully electromagnetic and include the perturbed electrostatic potential $\delta\phi$, perturbed parallel magnetic vector potential $\delta A_\parallel$, and perturbed parallel magnetic field $\delta B_\parallel$.

Table 2 lists the numerical resolutions used in these simulations. It is important to note that each code uses a different discretisation of the 5D space and most notably

Numerical resolution of hybrid KBM simulations			
	CGYRO	**GENE**	**GS2**
n_θ	32	32	32
n_r	64	64	64
n_ξ, n_v, n_λ	32	32	29
n_ϵ, n_μ, n_ϵ	8	16	16
n_{k_y}	64	64	64
$k_{y,\mathrm{min}}\rho_s$	0.01	0.01	0.01
L_x/ρ_s	166	166	166

Table 2: *Numerical resolution used in CGYRO, GENE and GS2 nonlinear simulations, with n_θ and n_r denoting the number of grid points in the parallel and radial direction, respectively. In CGYRO, n_ξ is the number of Legendre pseudospectral meshpoints in the pitch-angle space and n_ϵ is the number of generalized-Laguerre pseudospectral meshpoints. In GENE, n_v and n_μ are the number of grid points in the $v_\parallel$ and μ direction, respectively. In GS2, n_ϵ is the number of energy grid points and n_λ is the number of pitch-angles. L_x denotes the radial domain size, while $k_{y,\mathrm{min}}$ is the minimum k_y mode evolved in the simulation.*

different coordinate systems in velocity space §: CGYRO uses (χ, v), where $\chi = v_\parallel/v$ is the cosine of the pitch angle; GENE uses $(\mu, v_\parallel)$, where $\mu = v_\perp^2/(2B)$ is magnetic moment normalised by the species mass; and GS2 uses $(\lambda, \epsilon, \sigma)\|$, where $\lambda = v_\perp^2/(v^2 B)$, energy $\epsilon = m_s v^2/(2T_s)$ and $\sigma = v_\parallel/|v_\parallel|$.

A total of 64 toroidal modes are evolved to span the full range, $0.01 < k_y\rho_s < 0.63$, where modes are unstable (see Figure 2). At the minimum finite $k_y\rho_s$ (0.01) the toroidal mode number is $n = 2$. The radial box size, $L_x = j/(\hat{s}k_{y,\mathrm{min}})$, is set, using integer j, to 166 ρ_s. The velocity grids are set up to encompass a region up to $v_{\mathrm{max}} = 3v_{\mathrm{th,s}}$, where the thermal velocity of species s $v_{\mathrm{th,s}} = \sqrt{2T_s/m_s}$. Given the lack of an external source of momentum in STEP, we neglect equilibrium rotation though $\mathbf{E}\times\mathbf{B}$ shearing is considered in §3.

The radial resolution in these simulations is set to be sufficient to resolve the hybrid KBM instability¶, but is too coarse to resolve the subdominant MTM instability: MTMs require higher radial resolution due to their intrinsically multiscale nature as they include structures at ion Larmor scale in $k_y\rho_s$ and electron Larmor scale in $k_x\rho_s$. Here we focus

§ In gyrokinetics velocity space is 2D, involving the velocity component parallel to the magnetic field $v_\parallel$ and the magnitude of the perpendicular velocity component $v_\perp$, with the total velocity $v^2 = v_\parallel^2 + v_\perp^2$.
‖ The GS2 trapped velocity and parallel real space grids are tightly coupled, with the number of trapped pitch angles $n_{\mathrm{trap}} = n_\theta/2+1$ where n_θ is the number of parallel grid points. The total number of pitch angle grid points $n_\lambda = n_{\mathrm{trap}} + n_{\mathrm{pass}}$, where n_{pass} is the (unconstrained) number of passing pitch angles.
¶ Nonlinear simulations using CGYRO or GENE with the resolution in table 2 typically require approximately 3×10^5 CPU-hours on the ARCHER2 high performance computing system.

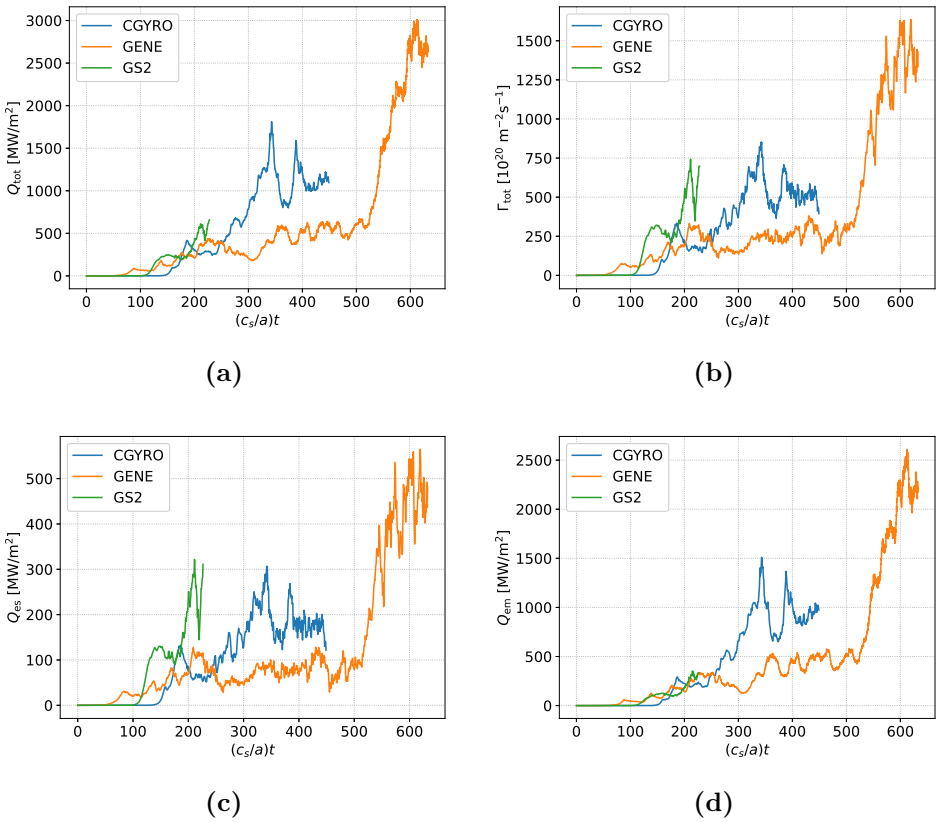

Figure 3: *Time trace from CGYRO, GENE and GS2 nonlinear simulations of (a) total heat flux, (b) total particle flux, (c) electrostatic and (d) electromagnetic contributions to the total heat flux. The electromagnetic heat flux is mainly from magnetic flutter associated with* $\delta A_\parallel$.

on the dominant hybrid-KBM instability, while the subdominant MTM instability is specifically addressed using higher radial resolution grids in §5. Attempting to resolve both modes simultaneously drastically increases the computational cost and appears to make no qualitative or quantitative change to the simulation results on the timescales considered here.

Figure 3 (a) and (b) shows time traces of the total heat and particle fluxes from nonlinear simulations using CGYRO, GENE and GS2. In all simulations the fluxes rise to very large values with no robustly steady saturation periods over the times simulated. The transport contributions from the electrostatic and electromagnetic channels are both substantial, as shown in Figure 3 (c) and (d). Arguably turbulence pseudo-saturates transiently at total heat flux values of approximately $Q_{\rm tot} \simeq 200$ MW/m^2 between $t \simeq 150\, a/c_s$ and $t \simeq 200\, a/c_s$. We note that this would correspond to a total power crossing the $q = 3.5$ surface $P_{\rm tot} > 100$ GW, which is orders of magnitude larger than the available heating power $P_{\rm surf} \simeq 500$ MW assumed for this STEP flat top operating point [11]. After this very short pseudo-saturated phase, the heat flux rapidly

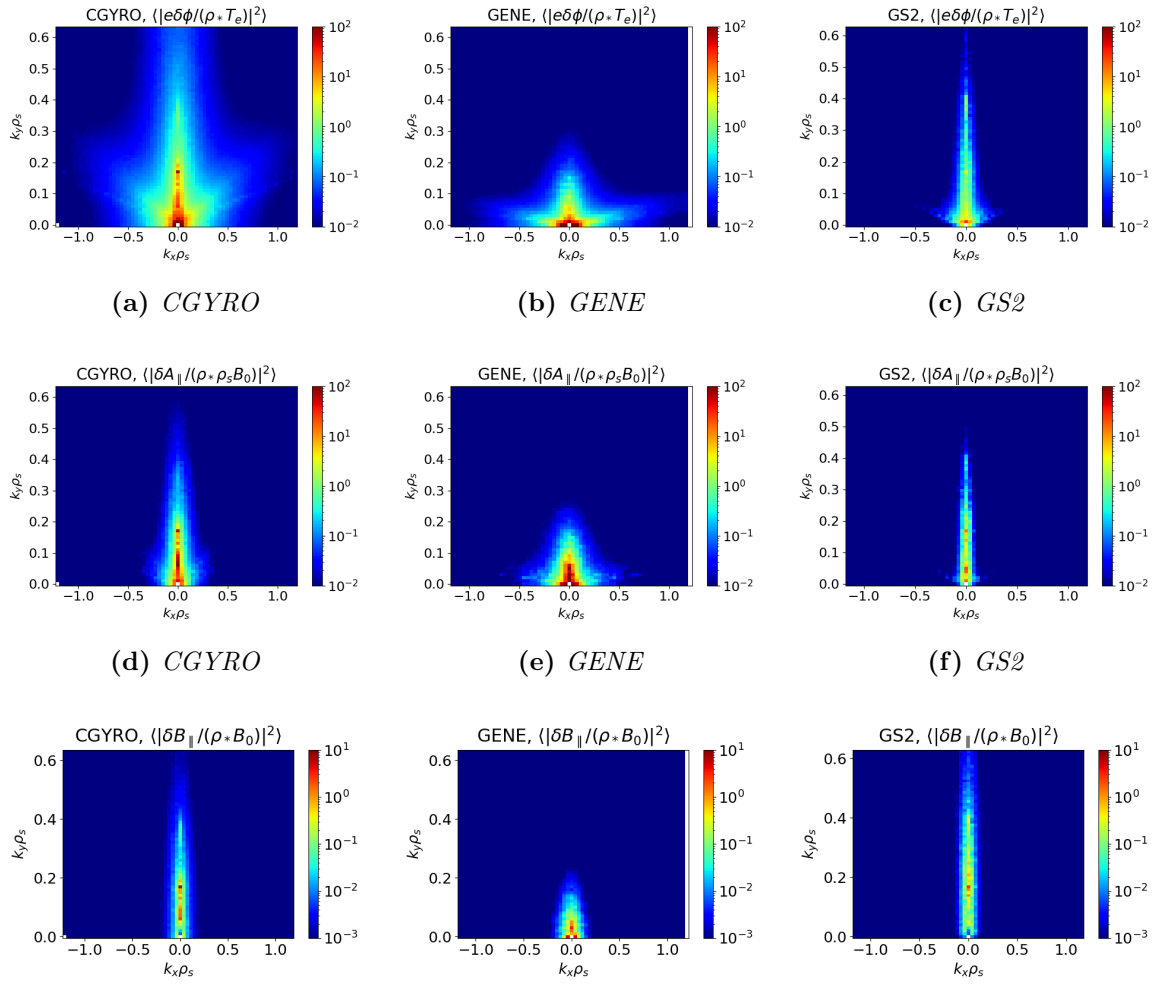

(a) *CGYRO* **(b)** *GENE* **(c)** *GS2*

(d) *CGYRO* **(e)** *GENE* **(f)** *GS2*

(g) *CGYRO* **(h)** *GENE* **(i)** *GS2*

Figure 4: *Time and θ averaged $\delta\phi$, $\delta A_\parallel$ and $\delta B_\parallel$ spectra from CGYRO [(a), (d) and (g)], GENE [(b), (e) and (h)] and GS2 [(c), (f) and (i)] nonlinear simulations. The time average is performed over the time interval $150 < (c_s/a)t < 200$ in all the three codes. The same color scale is used in all the spectra for an easier comparison, except for $\delta B_\parallel$ spectra where a smaller upper and lower color scale boundary is used ($\delta B_\parallel$ is smaller than $\delta\phi$ and $\delta A_\parallel$).*

grows to $Q_{\rm tot}$ values that exceed 1000 MW/m^2. There is a good qualitative agreement between the three codes, both in the very short pseudo-saturation phase and in the following evolution to yet larger fluxes.

The time and θ averaged $\delta\phi(k_x, k_y)$, $\delta A_\parallel(k_x, k_y)$ and $\delta B_\parallel(k_x, k_y)$ spectra are compared in Figure 4, where the time average is performed between $t = 150\, a/c_s$ and $t = 200\, a/c_s$. There is reasonable qualitative agreement between spectra from different codes, albeit with differences especially for the high k_y modes where CGYRO and GS2 find higher amplitudes than GENE, and for high k_x where the amplitude in $\delta\phi$ is lower

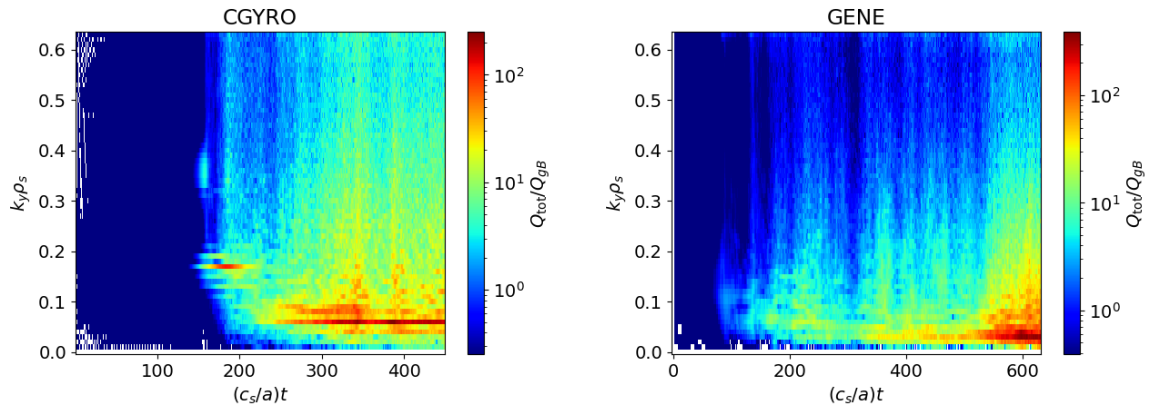

(a) **(b)**

Figure 5: *Time trace of the k_y resolved total heat flux spectrum from the CGYRO (a) and GENE (b) nonlinear simulation of Figure 3.*

in GS2 than in CGYRO and GENE. Mode at high k_y and k_x, however, do not contribute significantly to the turbulent heat fluxes, which agree reasonably well in this timeframe in Figure 3. Comparing the high k_x modes, we note that the amplitude of $\delta\phi$ is smaller in GS2 than in CGYRO and GENE, but turbulent transport is mainly driven by low k_x modes, where the agreement between the three codes is relatively good. The zonal ϕ and $A_\parallel$ components are larger in CGYRO and GENE than in GS2. We note that $\delta B_\parallel/B_0$ is consistently smaller than $e\delta\phi/T_e$ and $A_\parallel/(\rho_s B_0)$ in all three codes, and $\delta B_\parallel$ (like $\delta A_\parallel$) spectra are relatively narrow around $k_x = 0$. We highlight that the amplitude of the $\delta A_\parallel$ modes at low k_y values are relatively large in all three codes.

The time evolution of the k_y spectrum of the heat flux are shown in Figure 5 from CGYRO and GENE simulations. These indicate that the large fluxes at late times are mostly carried by low k_y modes, in a state where Figure 4 shows that the amplitudes of non-zonal modes exceed the amplitudes of zonal modes.

Snapshots of $\delta\phi$ and $\delta A_\parallel$ in real space are shown in Figure 6 from late high heat flux phases of the CGYRO and GENE simulations at $t = 400a/c_s$ and $t = 600a/c_s$ respectively. We note that both $\delta\phi$ and $\delta A_\parallel$ extend radially though the entire flux-tube domain and turbulence of such a character is not well modelled using the local approach. We note that turbulence of such a character questions the applicability of the local approach.

Convergence of these results is investigated by performing a set of CGYRO and GENE nonlinear simulations with a range of numerical resolutions given in table 3. Figure 7 shows that time traces of the total heat flux from these simulations agree very well, suggesting these local simulations are well resolved. We note in particular that increasing the size of the radial domain does not avoid large heat fluxes.

In brief summary, local gyrokinetic simulations neglecting equilibrium flow shear for the nominal parameters of a core flux surface of STEP-EC-HD evolve towards large

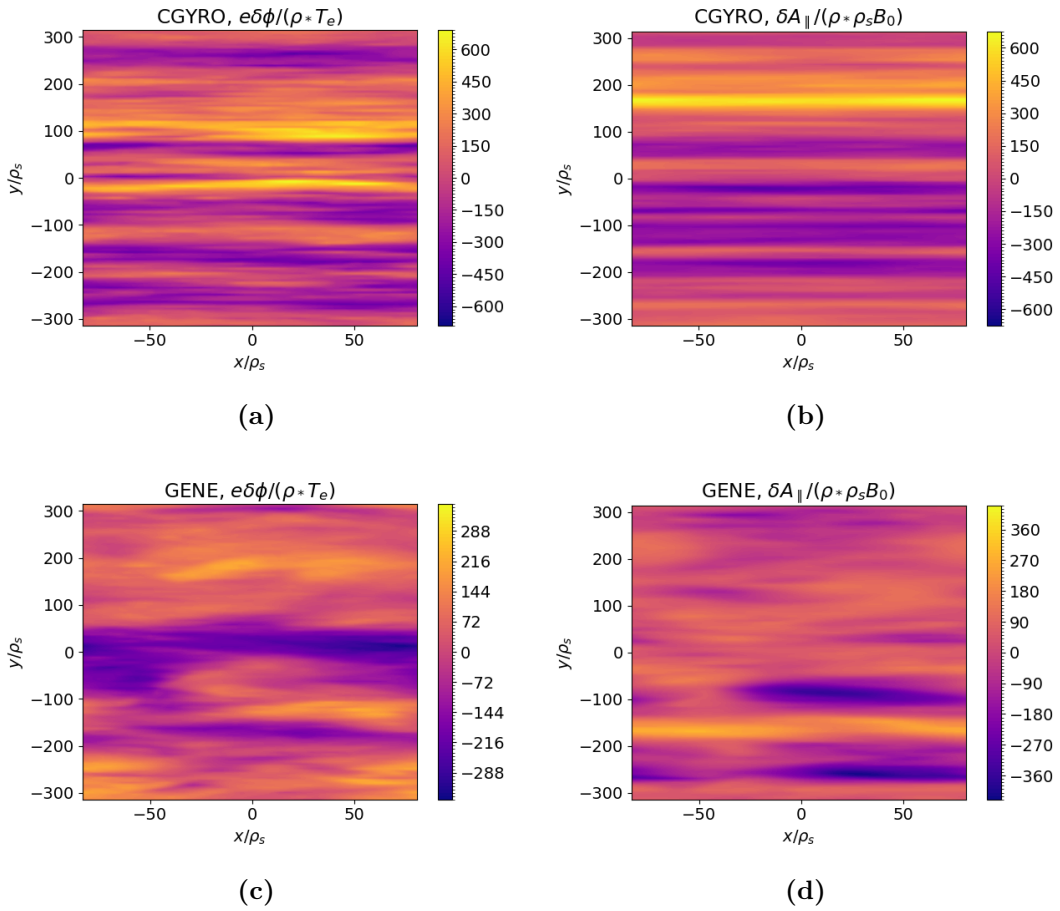

Figure 6: *Snapshot of $\delta\phi$ [(a) and (c)] and $\delta A_\parallel$ [(b) and (d)] from the CGYRO and GENE nonlinear simulations at $t = 400\,a/c_s$ and $t = 600\,a/c_s$, respectively. Snapshots of $\delta B_\parallel$ are similar to those of $\delta\phi$ and $\delta A_\parallel$.*

	CGYRO			**GENE**		
	Ref	**A**	**B**	**Ref**	**A**	**B**
n_θ	32	32	32	32	32	32
n_r	64	64	64	64	128	64
n_ξ, n_v	32	32	64	32	32	64
n_ϵ, n_μ	8	8	8	16	14	28
n_{k_y}	64	64	64	64	64	64
$k_{y,\min}\rho_s$	0.01	0.01	0.01	0.01	0.01	0.01
L_x/ρ_s	166	332	166	166	250	332

Table 3: *Numerical resolution used in the CGYRO and GENE convergence studies shown in Figure 7.*

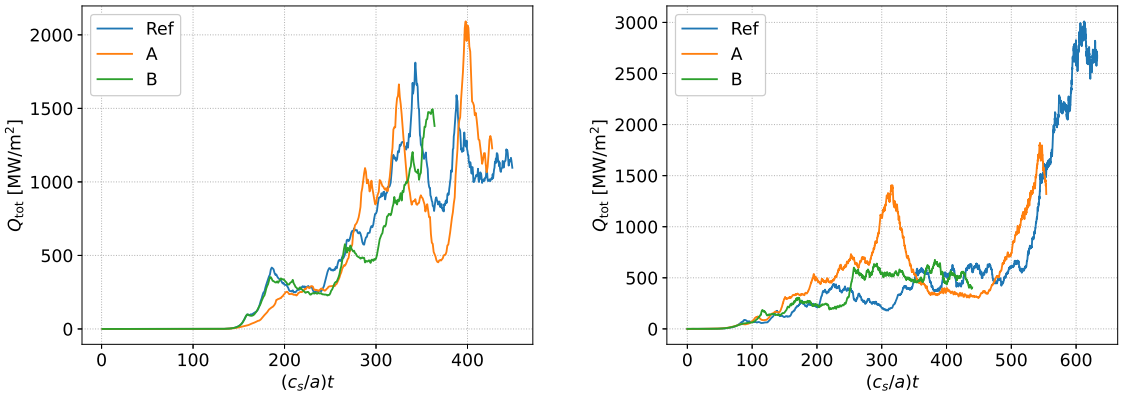

(a) *CGYRO* **(b)** *GENE*

Figure 7: *Time trace of the total heat flux from CGYRO (a) and GENE (b) nonlinear simulations with different numerical resolutions. Simulation parameters used in each case is listed in table 3.*

turbulent heat fluxes that are orders of magnitude larger than the available heating power. The predictions of local GK, as it stands (notably, without $\mathbf{E} \times \mathbf{B}$ shear), are clearly not compatible with the confinement assumptions made in the design of this STEP flat top operating point. The reproducibility of this result across three established local gyrokinetic codes lends support to the conclusion that these large heat fluxes (often reported in simulations of electromagnetic turbulence) are a robust prediction of local GK and are not a numerical artefact.

Importantly we cannot rule out the possibility that this prediction is simply due to the failure of the local GK approximation at small mode number: this possibility is supported by the fact that in all three codes the turbulent state becomes dominated by large amplitude low k_y modes that are very highly extended radially. Testing this potential failure of local GK will be addressed in the future using a global GK code, but this is beyond the scope of this paper.

In the following section, we will explore the effect of equilibrium flow shear.

3. Effect of the equilibrium flow shear

Sensitivity of the linear growth rate to the ballooning parameter $\theta_0 = k_x/(\hat{s}k_y)$ is a reliable indicator of a mode's susceptibility to equilibrium flow shear stabilisation. The linear analysis in [1] shows that the growth rate of the hybrid-KBM instability is highly sensitive to θ_0 and that the mode is stable for all θ_0 above a very small value. This indicates that hybrid-KBM turbulence should be very sensitive to flow shear, which has so far been neglected in our nonlinear simulations.

With no external momentum source from neutral beam injection in STEP

equilibria, the flow shearing rate γ_E is expected at the diamagnetic level (see e.g. [19]):

$$\gamma_E \simeq \gamma_{\rm dia} = \frac{1}{B}\Big(\frac{\partial \Psi}{\partial \rho}\Big)^2 \Big[\frac{1}{p_i n_i e(1+\eta_i)}\Big(\frac{\partial p_i}{\partial \Psi}\Big)^2 - \frac{1}{n_i e}\frac{\partial^2 p_i}{\partial \Psi^2}\Big] \tag{1}$$

where $\eta_i = L_n/L_{T_i}$ is the ratio of the density to the ion temperature gradient scale lengths, and p_i is the ion pressure. The value of γ_E at $\Psi_n = 0.49$ in STEP-EC-HD is approximately $\gamma_E \simeq 0.06 \pm 0.02\, c_s/a$, where the uncertainty is computed by taking the standard deviation over a radial interval $\Psi_n \in [0.48, 0.52]$ around the chosen surface.

We start by comparing nonlinear GENE and CGYRO simulations including equilibrium flow shear with $\gamma_E = 0.1\, c_s/a$, using the flow shear method recommended for each code. CGYRO favours a spectral approach to impose a radially periodic equilibrium flow [20], whereas GENE implements a radially constant $\mathbf{E}\times\mathbf{B}$ shearing rate by shifting the k_x grid in time [21,22]. GENE uses the wavenumber remapping method and includes continuous shearing in the nonlinear term detailed in [22] that had been neglected in earlier implementations of this approach. The diamagnetic shearing rate in Equation 1 is determined by the ion pressure profile and its gradients. Accordingly, a twofold effect is expected as pressure increases through the plasma discharge: on the one hand increasing $\mathrm{d}p_i/\mathrm{d}r$ will act to increase instability drives; and on the other rising diamagnetic flow shear and local shear at the outboard midplane will increasingly act to suppress turbulence.

Here we assess the impact of flow shear on fully developed turbulence at our chosen surface of the STEP-EC-HD flat-top, using CGYRO and GENE nonlinear simulations where the external flow shear is turned on only after the turbulence and fluxes have reached large amplitudes. Numerical convergence, which will be discussed further in §3.1, requires a large radial box width corresponding to $\Delta k_x \rho_s = 0.01$.

The time traces of the total heat flux from these simulations are shown in Figure 8, where external flow shear, included from $t = 300\, a/c_s$, triggers a sharp reduction in the heat flux in both codes. The heat flux decays more rapidly in GENE than in CGYRO, but at late times the saturated heat flux is comparable in both simulations. This is illustrated in Figure 8(b), where the error bars correspond to the standard deviation of the flux computed over the saturated phase of each simulation (after $t = 1400\, a/c_s$ and $t = 500\, a/c_s$ in CGYRO and GENE, respectively). The total saturated heat flux is approximately $Q_{\rm tot} \simeq 2$ MW/m^2, which corresponds to a power crossing the surface of $P_{\rm tot} \simeq 600$ MW. This is close to the total heat source of 500 MW assumed in STEP-EC-HD.

Whilst these results are promising, it is important to highlight that the quantitative heat flux prediction comes with a large uncertainty that will be discussed further in §3.1. Nevertheless, the results in Figures 3 and 8 indicate that equilibrium flow shear suppression of turbulent transport will be very important in these plasmas.

Figure 9 illustrates results from a scan to assess the sensitivity of the heat and particle fluxes to γ_E. In each simulation, the turbulence is allowed to develop large fluxes before the flow shear is switched on at $t = 300\, a/c_s$ so that the initial phase of these simulations is identical to that in Figure 8. At $\gamma_E = 0.05\, c_s/a$, both CGYRO

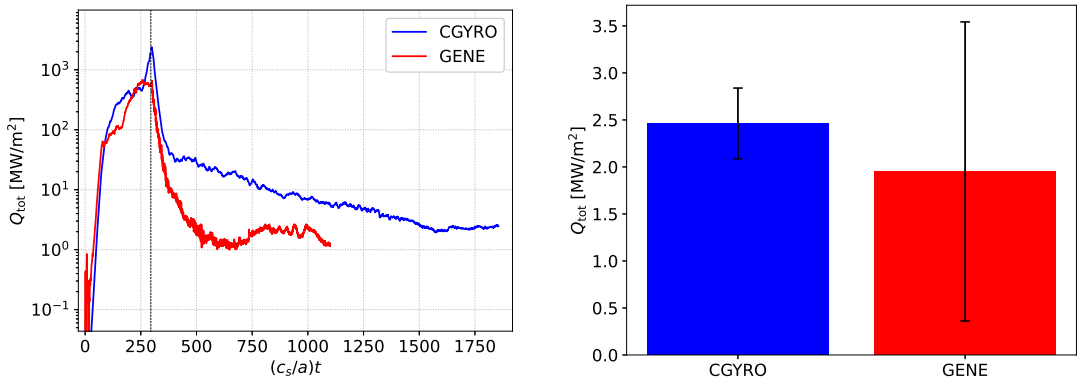

(a) **(b)**

Figure 8: *Time trace of the total heat flux (a) and saturated heat flux values (b) from CGYRO and GENE nonlinear simulations with flow shear activated at* $t = 300\, a/c_s$ *(*$\gamma_E = 0.1\, c_s/a$*). The dashed vertical line corresponds to the onset of the external flow shear in the simulations.*

and GENE predict a total heat flux larger than $Q_{\rm tot} \simeq 5$ MW/m^2 (corresponding to $P_{\rm tot} > 1.5$ GW), although the GENE simulation shows much stronger flow-shear suppression of the fluxes. Both the heat and particle fluxes decrease as γ_E is increased further. We note that both codes agree very well qualitatively on the flow-shear suppression of turbulent fluxes, and the flux predictions are within a factor of four of each other at $\gamma_E = 0.1\, c_s/a$ and $\gamma_E = 0.2\, c_s/a$. At $\gamma_E \gtrsim 0.1\, c_s/a$ the particle flux drops below $\Gamma_{\rm tot} \simeq 10^{20}$ m^{-2}s^{-1}, corresponding to a total particle flux of approximately 10^{22} s^{-1} crossing the chosen surface, which is comparable to the expected fuelling rate [+]. The electrostatic and electromagnetic contributions to electron heat flux, ion heat flux and particle flux are reported in Table 4. The electromagnetic electron heat flux gives the largest contribution to the total heat flux at all the γ_E values considered here. The electromagnetic particle flux is significantly larger than the electrostatic one in GENE simulations with $\gamma_E \geq 0.1\, c_s/a$, while the two contributions are comparable in CGYRO simulations as well as in GENE simulation with $\gamma_E = 0.05\, c_s/a$. The values of the effective total heat and particle diffusivities, $\chi_{\rm tot} = Q_{\rm tot}/(\sum_s n_s \partial T_s/\partial r)$ and $D_{\rm tot} = \Gamma_{\rm tot}/(\partial n/\partial r)$, are also reported in table 4 for each nonlinear simulation.

[+] A pellet fuelling rate of 7.4 $\times 10^{21}$ particles/s is used in the modelling of the STEP-EC-HD flat-top, based on an assumption that the particle confinement time $\tau_p \sim 4.5\tau_E$ (as it is typical in JET). This results in $\tau_p \sim 16$ s. Assuming the same confinement time for helium ash gives a saturated helium abundance of about 9% and higher particle confinement would severely degrade fusion performance due to the core accumulation of helium ash.

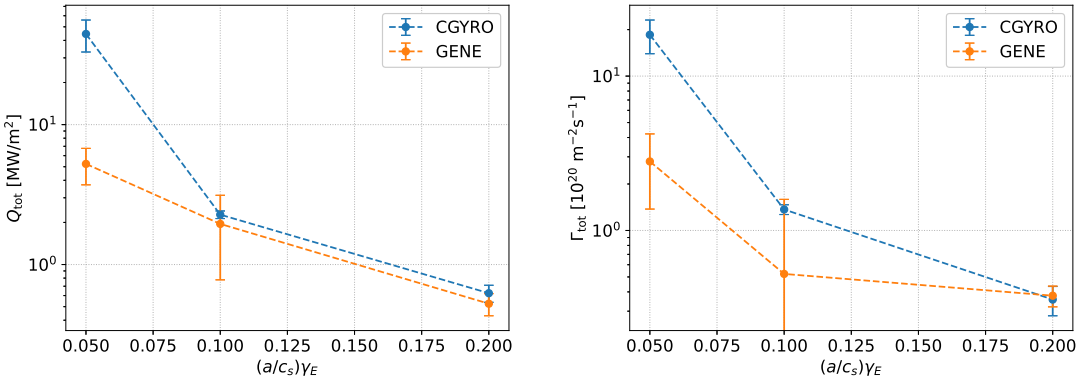

(a) **(b)**

Figure 9: *Total heat flux (a) and particle flux (b) from the saturated phase of CGYRO and GENE nonlinear simulations at different values of γ_E. The error bars are computed from standard deviations of the fluxes in the saturated phase. The flow shear is turned on at $t \simeq 300\, a/c_s$ in all of the simulations.*

	CGYRO			**GENE**		
$(a/c_s)\gamma_E$	0.05	0.10	0.20	0.05	0.10	0.20
$Q_{\mathrm{e,es}}$	2.2 (± 0.5)	0.19 (± 0.02)	0.05 (± 0.01)	0.32 (± 0.27)	0.05 (± 0.26)	0.02 (± 0.01)
$Q_{\mathrm{i,es}}$	3.9 (± 0.9)	0.32 (± 0.03)	0.11 (± 0.02)	0.45 (± 0.38)	0.04 (± 0.28)	0.03 (± 0.28)
$Q_{\mathrm{e,em}}$	35.9 (± 9.6)	1.57 (± 0.11)	0.41 (± 0.06)	4.01 (± 1.13)	1.74 (± 1.01)	0.39 (± 0.08)
$Q_{\mathrm{i,em}}$	2.4 (± 0.6)	0.19 (± 0.01)	0.04 (± 0.01)	0.44 (± 0.12)	0.12 (± 0.06)	0.09 (± 0.01)
Γ_{es}	9.6 (± 2.4)	0.66 (± 0.07)	0.20 (± 0.05)	1.20 (± 0.96)	0.09 (± 0.91)	0.08 (± 0.04)
Γ_{em}	8.9 (± 2.4)	0.71 (± 0.05)	0.16 (± 0.03)	1.60 (± 0.53)	0.43 (± 0.26)	0.30 (± 0.03)
χ_{tot}	87	4.4	1.2	10.2	3.8	1.0
D_{tot}	10.1	0.74	0.19	1.52	0.28	0.21

Table 4: *Electrostatic and electromagnetic contributions to heat fluxes in MW/m^2 and to particle fluxes in $10^{20} m^{-2} s^{-1}$ from CGYRO and GENE simulations with equilibrium flow shear activated at $t = 300\, a/c_s$. Effective total heat diffusivity χ_{tot}, and effective particle diffusivity D_{tot}, are also reported in units of m^2/s. All fluxes and errors in parentheses are computed from time averages and standard deviations in the saturated phase.*

3.1. Challenges simulating flow shear in STEP-relevant plasmas

Although we have clear evidence to suggest that flow shear has a strongly suppressing impact on the turbulence, it is important to highlight the caveats and challenges associated with these simulations.

3.1.1. Numerical implementation of flow shear The cross-code comparison with GENE and CGYRO has revealed some large differences in the modelled impact of flow shear on fluxes especially at low γ_E, e.g., the simulations with $\gamma_E = 0.05\, c_s/a$ in Figure 9. This is not surprising and is likely at least partly due to the different numerical implementations of flow shear in CGYRO and in GENE (we have tested this using CGYRO with an optional implementation of flow shear based on wavenumber remapping [21] that neglects the nonlinear shearing term [22]: nonlinear simulations for STEP using this flow shear implementation in CGYRO are found in Appendix A to give very similar results to comparable GENE simulations that also exclude the nonlinear shearing term). This work highlights the value and importance of multi-code comparisons to point out research priorities, especially when accurate flux predictions are required in new plasma regimes where no experiments are available for validation.

3.1.2. Possible failure of the local approximation The dependence of γ_{KBM} on θ_0 is very sharp, with a narrow instability window in θ_0 (see Figure 15 of [1]). This poses resolution challenges for nonlinear simulations because it requires large radial box sizes in order to resolve sufficiently finely in k_x and θ_0. For the equilibrium considered here, at the k_y of the peak heat flux, $k_y\rho_s = 0.04$, we found that $\Delta k_x\rho_s \simeq 0.01$ corresponds to a θ_0 resolution $\Delta\theta_0 \simeq 0.06\,\pi$. This resolution was both: (i) sufficient to resolve the strong θ_0 dependence of the linear growth rate at $k_y\rho_s = 0.4$; and (ii) necessary to achieve convergence in both GENE and CGYRO. However, running local simulations in a such a large radial box pushes the validity of the local approximation. In particular, the value of $\Delta k_x\rho_s = 0.01$ corresponds to a radial flux tube domain size of $L_x \simeq 600\,\rho_s \simeq 3$ m, which is larger than the minor radius of the device*.

3.2. Summary of flow shear findings

Local GK simulations with CGYRO and GENE indicate that equilibrium flow shear should have a strongly suppressing impact on turbulent transport at this surface in STEP-EC-HD (see Figures 3 and 8), and with flow shear close to the diamagnetic level the resulting heat flux is in the same ballpark as the anticipated heat source. While there are quantitative disagreements between codes (most notably at $\gamma_E = 0.05\ c_s/a$), this may at least in part be attributed to different numerical implementations of flow shear. Our local simulations with flow shear have required using radially extended domains

* Nevertheless, we note previous work where local gyrokinetic simulations in a radially extended domain larger than the minor radius were used to model ITG turbulence in MAST, finding turbulence properties that were remarkably close to fluctuation measurements made using Beam Emission Spectroscopy [23].

where the local approximation may be more questionable, and it would be interesting to explore in the future whether local GK using a continuous-in-time approach to flow shear, like that outlined in [24], improves numerical convergence especially in narrower radial domains (i.e. at higher values of Δk_x). If the turbulent eddies are excessively extended radially, the local approximation may start to break down as global equilibrium profile variation effects become important. Our results motivate future research to perform global simulations, that must include $\delta B_{\parallel}$ to capture the hybrid-KBM, to seek higher fidelity predictions of transport fluxes in STEP-like plasmas. A key future priority will also be to validate these types of calculations in detail against data from experiments, especially from higher β plasmas getting closer to STEP-like regimes. The available validation data set will improve considerably following the planned enhancements for MAST-U to upgrade the Neutral Beam Injection heating system and install an Electron Bernstein Wave heating and current drive capability.

Transport fluxes in STEP-EC-HD are clearly sensitive to flow shear, and in the next section we consider the sensitivity to other local equilibrium parameters.

4. Sensitivity to local parameters

The previous section suggest that the hybrid KBM instability can generate substantial transport even in the presence of $\mathbf{E} \times \mathbf{B}$ shear flows. This motivates the investigation of the dependence of the heat and particle flux on various local parameters, such as pressure gradient, β_e, q and $\hat{s}$. The analysis presented here is carried out by using CGYRO where a single local equilibrium parameter is varied. Throughout this section we have neglected sheared equilibrium flows, which would complicate the dependencies and may reduce fluxes if they were included.

4.1. Sensitivity to linear drive terms at constant β' (inconsistent)

We first consider a set of simulations carried out at different values of pressure gradient (we scale both the electron and ion temperature gradients whilst keeping the density gradients fixed) $a/L_p \in \{2.73, 2.33, 1.93, 1.53\}$. All other local equilibrium parameters were held fixed including β' (which is inconsistent but preserves the local equilibrium magnetic field geometry). Since the pressure gradient is the main drive of the hybrid KBM instability, the saturated total heat flux is expected to decrease as pressure gradient is reduced and this is confirmed in Figure 10(a). Q_{tot} has a very stiff dependence on a/L_p and decreases by more than two orders of magnitude when a/L_p is reduced by less than 20% with respect to its nominal value. The heat flux then decreases slightly from $a/L_p = 2.3$ to $a/L_p = 1.9$ and becomes negligible at $a/L_p = 1.53$.

4.2. Sensitivity to linear drive terms varying β' (consistent)

Here we repeat the above scan in pressure gradient, but setting β' to be consistent with a/L_p. This ensures the local equilibrium magnetic geometry is modified consistently

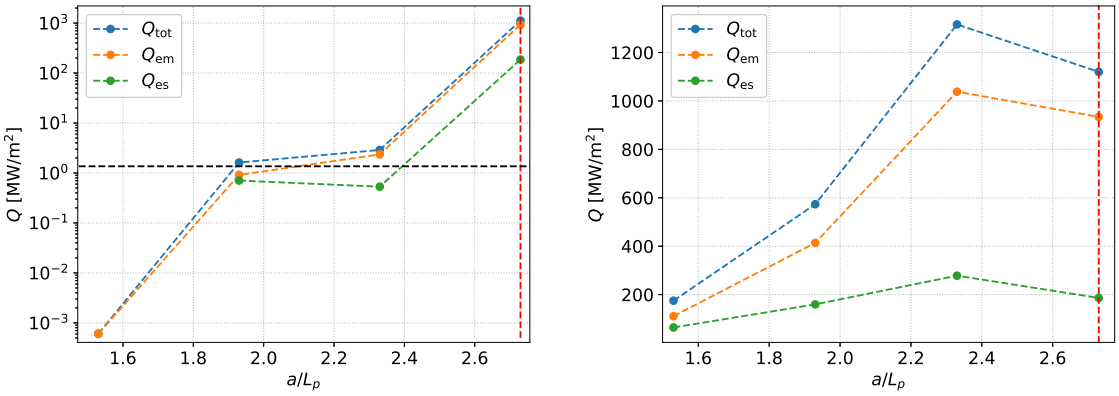

(a) *Constant β' value.* **(b)** *Varying β' value.*

Figure 10: *Total, electromagnetic and electrostatic saturated heat flux value from CGYRO nonlinear simulations at various values of a/L_p (varying the electron and ion temperature gradients). In (a) the value of β' is kept constant at the original equilibrium value when varying a/L_p, while in (b) the value of β' is varied consistently with a/L_p. Note the logarithmic y-axis scale in (a), while in (b) this is linear. The dashed vertical line denotes the reference value of a/L_p. The horizontal dashed line in (a) corresponds to the heat flux that would be driven across the chosen surface at steady-state from the total assumed heat source in STEP-EC-HD.*

with the local pressure gradient through the scan. Figure 10(b) shows the saturated heat flux value from these simulations. The heat flux dependence on a/L_p is much weaker in this case, particularly near the nominal value. The heat flux decreases from $a/L_p = 2.3$ to $a/L_p = 1.5$, but it remains very large ($Q_{\text{tot}} > 200$ MW/m^2) and substantially higher than the maximum steady state flux available from the expected heat source in STEP-EC-HD. The dramatic difference between Figures 10(a) and (b) is due to the fact that in (b) the reduced linear drive at lower pressure gradient drive is largely off-set by a loss of β' stabilisation (negative local magnetic shear and magnetic drifts are more favourable for stability at higher β' [**?**, 25], which is also associated with the onset of internal transport barriers [26]). As shown in [1], high β' has a strong linearly stabilising influence on the hybrid KBM on this surface in STEP-EC-HD. A transport steady state consistent with the available heating source in STEP-EC-HD cannot easily be achieved on this surface simply by reducing the reference pressure gradient. We also note that our GK analysis has neglected α particles that should impact on turbulence in the flat-top burning plasma equilibrium (α particles will interact directly with the turbulence and enhance the plasma pressure). A future work will explore the influence of fast α particles.

This work highlights the need for further development of the STEP-EC-HD plasma scenario and for systematic studies over the available parameter space, though these lie beyond the scope of the current study.

4.3. Sensitivity to β_e varying β' (consistent)

We focus now on the effect of β by performing nonlinear CGYRO simulations♯ at several values of β_e, varying β' consistently. Figure 11 shows the saturated total heat and particle fluxes from nonlinear simulations at different values of β_e.

At $\beta_e < 0.025$, the particle and heat transport is mainly electrostatic and is driven by an ITG/TEM instability (the KBM instability couples to an ITG/TEM instability at low β as noted in [1]). We note that the electrostatic heat and particle fluxes remain above 100 MW/m^2 and 10^{22} particles/(m^{2}s) even at $\beta_e = \beta_{e,\mathrm{ref}}/4$ (presumably due to weakened β' stabilisation). This scan suggests turbulent transport could challenge access to the burning flat-top through the lower β phase during the I_p ramp-up, although considerably more detailed self-consistent scenario modelling is clearly required before firmer conclusions can be drawn.

At the higher value $\beta_e = 0.16$, electromagnetic contributions dominate transport and the total heat flux drops considerably to $Q_{\mathrm{tot}} \simeq 2$ MW/m^2, corresponding to a power crossing the surface of approximately $P_{\mathrm{tot}} \simeq 600$ MW. This is a consequence of increased β' stabilisation of the hybrid KBM, leaving the MTM (with linear growth rates hardly affected by β' [1]) surviving as the dominant instability. This $\beta_e = 0.16$ operating point would have considerably more favourable transport than the reference local equilibrium at $\beta_e = 0.09$, if it could be accessed through a route that avoided prohibitive transport losses from hybrid-KBMs. However, a global equilibrium with this local β_e would likely exceed the limiting β for effective control of Resistive Wall Modes, as noted in [1].

Figure 12 is an $\hat{s} - \alpha$ diagram (where $\alpha = -Rq^2\beta'$) showing the ideal $n = \infty$ ballooning boundary and how the local equilibrium point moves in this space over the scan. The equilibrium points at $\beta_e = 0.02$ and $\beta_e = 0.16$ are further from the stability boundary then the reference equilibrium at $\beta_e = 0.09$, suggesting a weakening the role for KBMs that would be consistent with reduced heat and particle fluxes.

4.4. Sensitivity to q and $\hat{s}$

Finally, we analyse the effect of local safety factor and magnetic shear. Figure 13 shows the saturated heat flux from a set of CGYRO nonlinear simulations with different values of q and $\hat{s}$. Consistent with the linear predictions of [1], we find that the heat flux decreases as q increases or $\hat{s}$ decreases. In particular, we note that the heat flux drops by almost two orders of magnitude when q is increased from $q = 3.5$ (nominal value) to $q = 4.0$, while the maximum growth rate decreases by approximately a factor of two. On the other hand, the heat flux decrease is less stiff (but still noticeable) when the magnetic shear is decreased. We can gain some important intuition for both of these results by looking at the ideal ballooning stability in the $\hat{s} - \alpha$ plane (see Figure 12):

♯ Numerical resolutions were chosen to properly resolve the linear spectrum of the dominant instability (see [1]). In particular, the simulations with $\beta_e = 0.02$ and $\beta_e = 0.005$ are carried out with $n_{k_y} = 128$ and $n_r = 64$, while the simulation with $\beta_e = 0.16$ is carried out with $n_{k_y} = 64$ and $n_r = 256$.

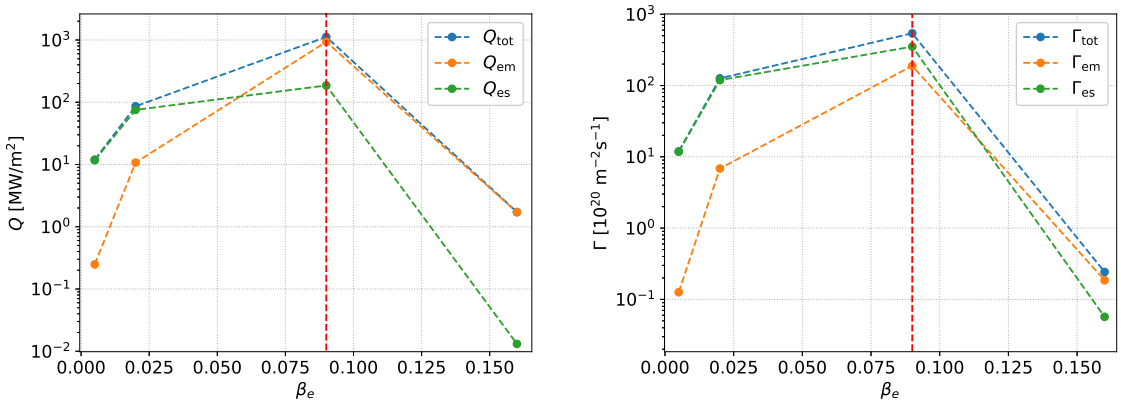

(a) *Heat flux* **(b)** *Particle flux*

Figure 11: *Total heat (a) and particle (b) fluxes from CGYRO nonlinear simulations at various values of β_e with β' varying consistently. The dashed vertical line denotes the reference value of β_e.*

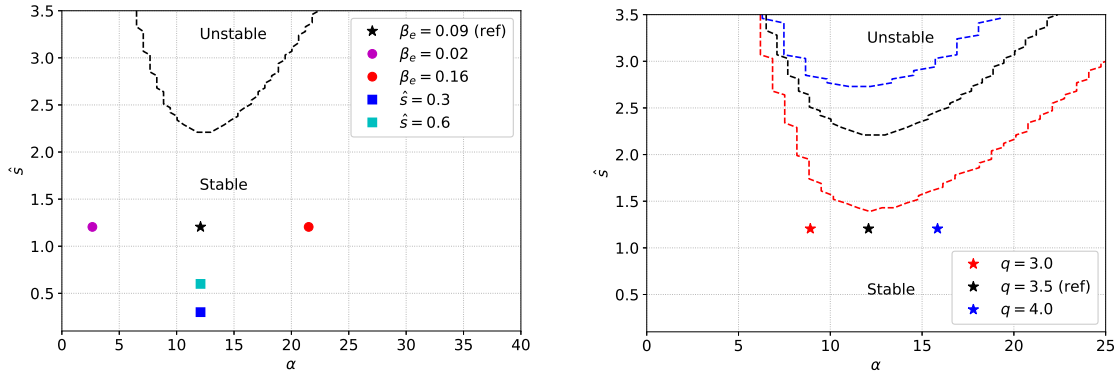

(a) **(b)**

Figure 12: *Ideal ballooning stability boundary in the $\hat{s} - \alpha$ plane of STEP-EC-HD. Panel (a) shows the position in the $\hat{s} - \alpha$ plane of the reference equilibrium and various cases with different values of β_e (round markers) and $\hat{s}$ (square markers). Panel (b) shows the ideal ballooning boundary for $q = 3.0$, $q = 3.5$ and $q = 4.0$ cases.*

lowering $\hat{s}$ moves the equilibrium further into the stable $\hat{s} - \alpha$ region, while raising q moves the unstable region to higher shear values and increases significantly the distance between the equilibrium point and the ideal ballooning stability boundary (consistent with lower fluxes at $q = 4.0$). Vice versa, lowering q moves the unstable region to smaller shear values, which is consistent with larger fluxes at $q = 3.0$. In summary, lowering $\hat{s}$ or raising q increases the distance from the operating point to the ideal ballooning stability boundary. These results therefore motivate a simple strategy for future exploitation to design equilibria with lower turbulent transport: varying the key equilibrium actuators

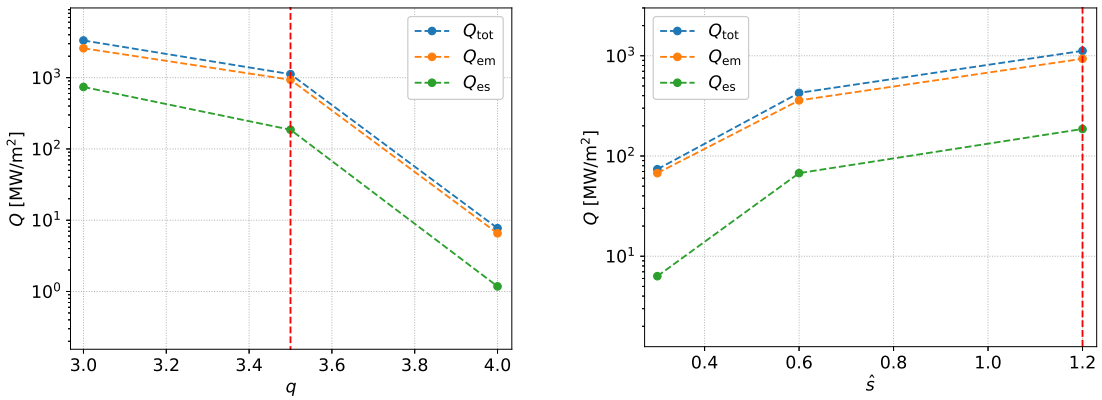

Figure 13: *Total, electrostatic and electromagnetic saturated heat flux value from CGYRO nonlinear simulations at three different values of safety factor (a) and magnetic shear (b). The red dashed vertical line denotes the nominal value.*

in the problem (e.g. shaping and profiles) and seek to maximise distance from the ideal ballooning boundary to reduce the impact of the hybrid KBM on transport.

5. The role of the subdominant MTM instability

Results in §3 show that the heat flux driven by the hybrid KBM instability can be significantly reduced by equilibrium flow shear. The subdominant MTM instability, linearly characterised in [1], however is resilient to flow shear, and is expected to become important when the hybrid-KBM is suppressed. As shown in [1], the hybrid KBM instability can be artificially suppressed by simply removing $\delta B_{\parallel}$ from the GK system of equations (so only $\delta\phi$ and $\delta A_{\parallel}$ are evolved), leaving the MTM as the surviving dominant instability in the reduced system. This artificial suppression of the hybrid mode provides a way to study MTM-only-driven turbulence.

We have adopted this approach to perform a dedicated nonlinear study of MTM turbulence on the reference surface in STEP-EC-HD. While it is unphysical to neglect $\delta B_{\parallel}$, this study is nevertheless of considerable interest because (i) MTMs have been demonstrated to be unstable and even dominant over an extended range of binormal scales in various conceptual designs of fusion power plants based on the ST [3, 27, 28], (ii) MTMs may be important where the hybrid-KBMs is suppressed (e.g. the high β, β' local equilibrium in Figure 11 or on surfaces analysed in [27]), or in other radial surfaces in STEP-EC-HD (e.g. at the pedestal) and (iii) MTMs have been demonstrated to have significant impacts on transport in other devices [29–34] and are consistent with pedestal magnetic fluctuation measurements in several experiments [31, 35–41].

The computational cost of modelling low k_y MTMs with conventional gyrokinetic codes is challenging due to the multiscale nature of the mode: $\delta\phi$ is highly extended

Numerical resolution of MTM simulations		
	CGYRO	**GENE**
n_θ	32	32
n_r	512	512
n_ξ, n_v, n_λ	32	32
n_ϵ, n_μ	10	16
n_{k_y}	16	16
$k_{y,\min}\rho_s$	0.021	0.021
L_x/ρ_s	158	156

Table 5: *Numerical resolution of CGYRO and GENE nonlinear simulations of the subdominant MTM instability, where $\delta B_\parallel$ is artificially removed. The parameters n_θ and n_r denotes the number of grid points in the parallel and radial direction, respectively. In CGYRO, n_ξ is the number of Legendre pseudospectral meshpoints in the pitch-angle space and n_ϵ is the number of generalized-Laguerre pseudospectral meshpoints. In GENE, n_v and n_μ are the number of grid points in the $v_\parallel$ and μ direction, respectively. L_x denotes the radial domain size, while $k_{y,\min}$ is the minimum k_y mode evolved in the simulation.*

in the field-line-following coordinate θ, which accommodates high radial wavenumbers, while $\delta A_\parallel$ is localised in θ and radially extended. Computational cost and difficulties in achieving saturation have limited the number of studies of saturated MTM driven turbulence in the literature [29, 30, 34].

Here we gauge the potential transport relevance of MTMs by performing nonlinear simulations with CGYRO and GENE artificially neglecting $\delta B_\parallel$, using the numerical resolutions given in Table 5. Figure 14 (a) shows the time traces of the total heat flux and demonstrates good agreement between codes that the MTM-driven heat flux saturates at a negligible level, $Q_{\rm tot} < 0.005$ MW/m^2. The heat flux is entirely electromagnetic and almost entirely in the electron channel, in agreement with MTM previous gyrokinetic simulations [29, 30]. Furthermore, MTMs drive effectively vanishing particle transport as expected for any electron driven instability that is insensitive to inclusion of the non-adiabatic ion response [42]. Zonal fields [7, 34] and local temperature flattening [43], are found to play a role in saturating this MTM instability at negligible heat flux values (see Appendix B). Figure 14 (b) shows time traces of the ratio of the non-zonal to the zonal $\delta A_\parallel$ mode amplitudes, demonstrating that zonal fields dominate in both codes and suggesting that they are likely to be important for saturation. ††.

Figure 15 shows the $\delta\phi$ and $\delta A_\parallel$ spectra from CGYRO and GENE simulations, again demonstrating that both $\delta\phi$ and $\delta A_\parallel$ non-zonal mode amplitudes are significantly

††Note that including an appropriate parallel dissipation scheme was found to be essential to avoid runaway nonlinear MTM fluxes [3], due to the onset of dominant unphysical numerical instabilities with grid-scale oscillations in the parallel direction. This prompted an improvement to the parallel dissipation scheme in CGYRO, implemented at commit `399deb4c`, that has been used in all of the simulations in this paper.

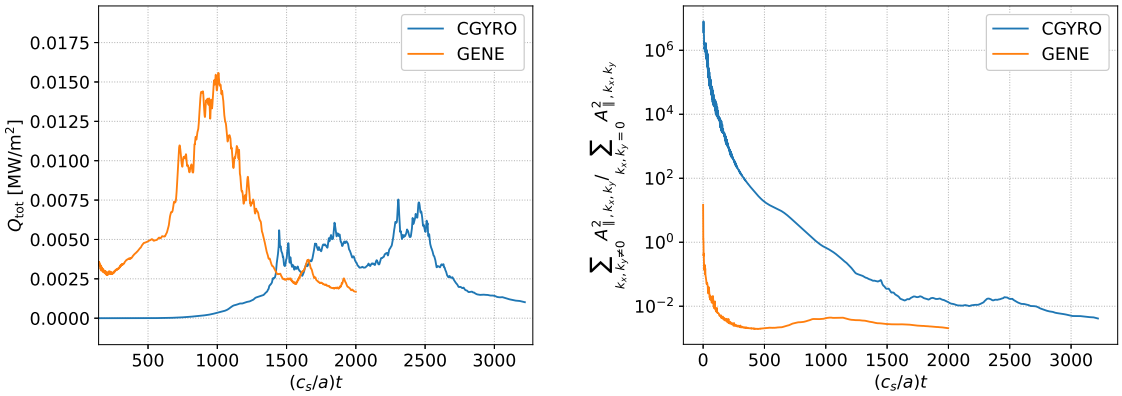

(a) **(b)**

Figure 14: *(a) Time trace of the total heat flux from CGYRO and GENE nonlinear simulations with $\delta B_\parallel = 0$ (MTM instability). (b) Time trace of the non-zonal to zonal $\delta A_\parallel$ mode amplitudes ratio from the same simulations.*

smaller than the corresponding zonal amplitudes. The spectra from CGYRO and GENE are qualitatively and quantitatively similar. In Figure 16, we show a snapshot of $\delta\phi$ and $\delta A_\parallel$ in real space at the intersection between the flux-tube with the outbpoard midplane, from the saturated states of CGYRO and GENE simulations. In both simulations, $\delta\phi$ is characterised by radially narrow structures, whilst $\delta A_\parallel$ exhibits streamers that are more extended in the radial direction. These are typical structures of MTM turbulence [29–34].

MTMs, previously identified from linear studies as potential drivers of significant electron heat transport in conceptual ST power plants [2, 3, 27], appear to make an insignificant contribution to transport on this particular mid-radius surface in STEP-EC-HD. We cannot exclude the possibilities (i) that MTM transport may dominate that from hybrid-KBMs under different local equilibrium conditions, and (ii) that multi-scale interactions between MTMs and hybrid KBMs may be significant; these are important avenues to be explored.

6. Conclusions

This paper presents the first nonlinear gyrokinetic simulations of turbulence and transport in the core of a conceptual STEP plasma reference flat-top operating point. Local nonlinear simulations were performed at the $q = 3.5$ surface (where $\psi_n = 0.49$) of the flat-top operating point STEP-EC-HD using three different well-established local gyrokinetic codes.

All codes robustly predict that the hybrid KBM [1], which requires inclusion of $\delta B_\parallel$ for instability, drives very high heat fluxes in all channels; in the absence of equilibrium flow shear the total heat flux is orders of magnitude larger than the available heating

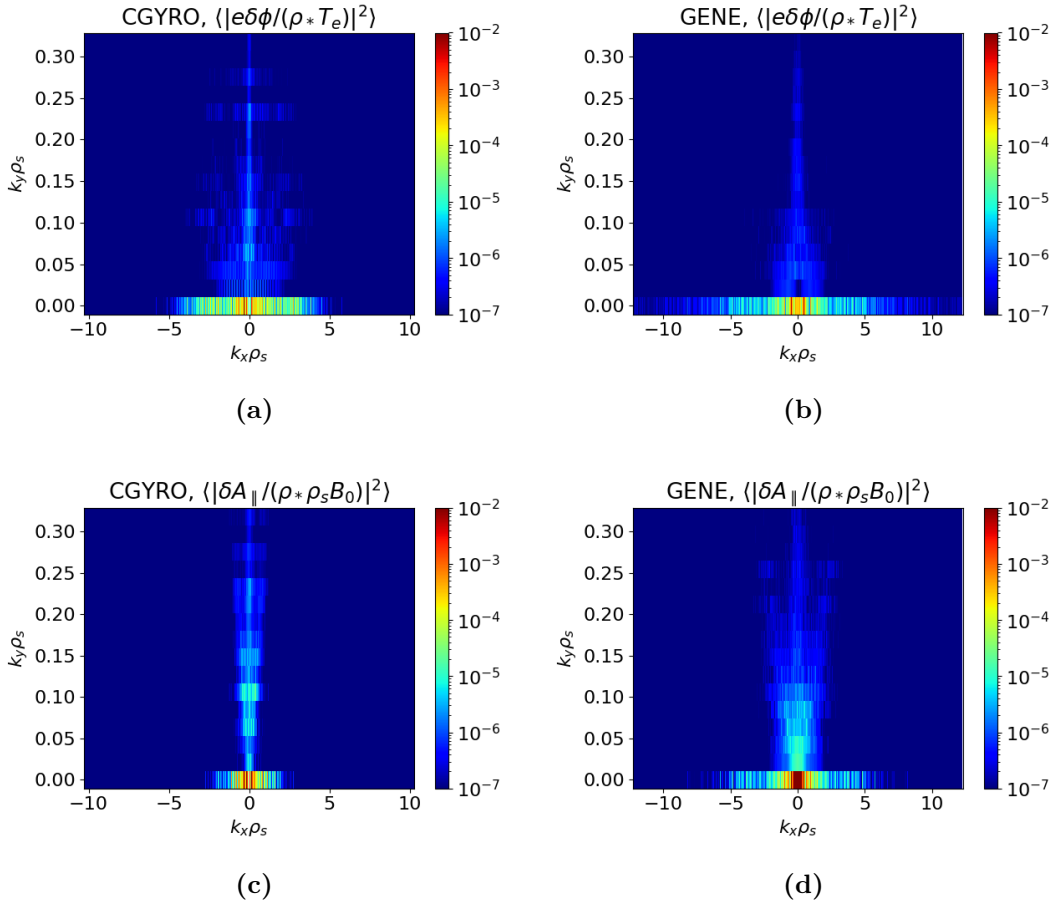

Figure 15: *Time and θ averaged spectra of $\delta\phi$ and $\delta A_\parallel$ from CGYRO [(a) and (c)] and GENE [(b) and (d)] nonlinear simulations with $\delta B_\parallel = 0$ (subdominant MTM instability). The time average is taken in the saturated phase. The same color scale is used in all the spectra for an easier comparison.*

power. Impressive cross-code agreement strongly supports that the large transport fluxes arise as a robust prediction of local nonlinear gyrokinetic model, and are not due to a numerical artefact. Simulations where the fluxes grow to large values are generally dominated by radially highly extended turbulent eddies at low k_y that may challenge the validity of the local equilibrium approximation. Higher fidelity modelling of such turbulence may require improvements to the local gyrokinetic model to include global and/or other higher order effects. These aspects should be explored in future research.

Turbulence from hybrid-KBMs is found to be extremely sensitive to equilibrium flow shear, and γ_E is critical in determining the saturation level. When γ_E is set at the same order as the diamagnetic flow shear, the total turbulent heat flux from hybrid-KBMs falls by orders of magnitude and becomes comparable with the total heating power assumed for the STEP-EC-HD flat-top operating point. This extreme sensitivity to flow shear introduces large uncertainty in the expected level of the turbulent transport.

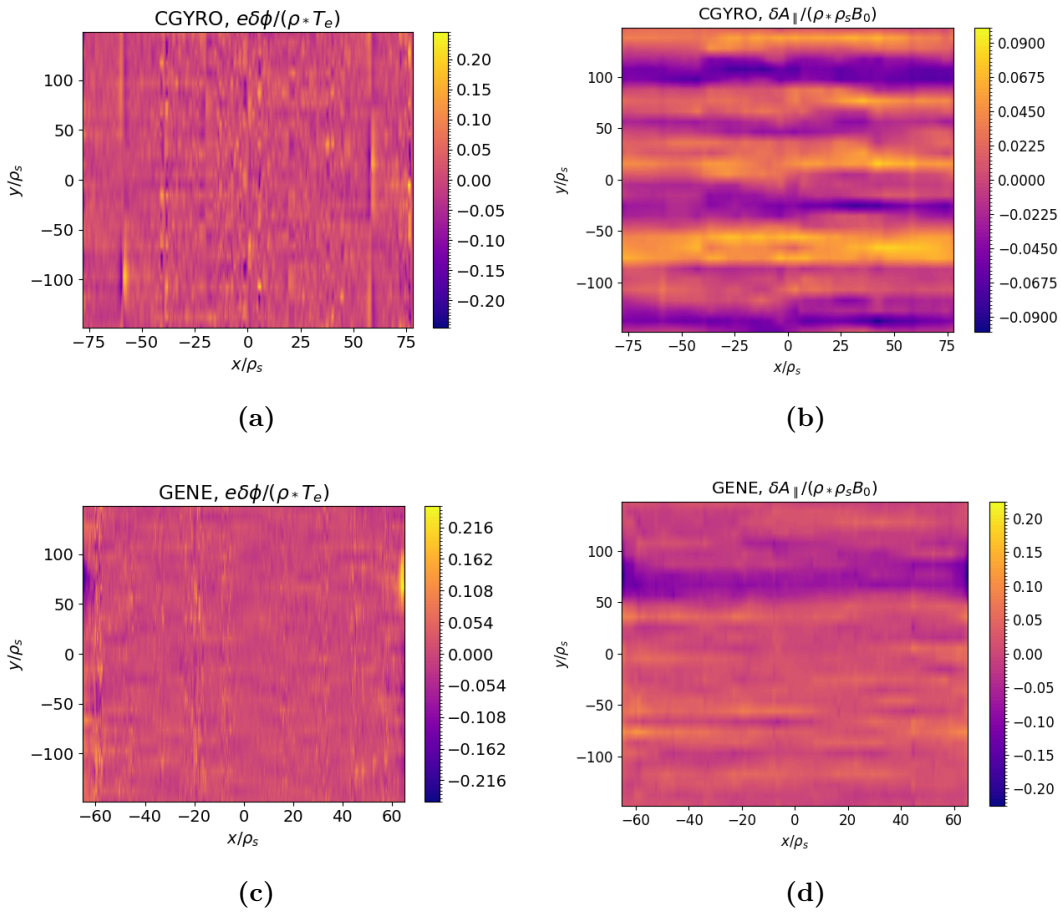

Figure 16: *Snapshot of $\delta\phi$ [(a) and (c)] and $\delta A_\parallel$ [(b) and (d)] from the CGYRO (top row) and GENE (bottom row) nonlinear simulations with $\delta B_\parallel = 0$. The zonal component is removed.*

Nonlinear scans were performed neglecting flow shear, to explore the sensitivity of hybrid-KBM transport fluxes to local equilibrium parameters, including: temperature gradient; β_e; q; and $\hat{s}$. Decreasing the temperature gradient via commensurate reductions in a/L_{T_e} and a/L_{T_i} with all other parameters constant *including* β' (i.e. pressure gradient is not varied consistently) was found to reduce the heat flux driven by the hybrid KBM considerably. The reduction in transport at lower temperature gradient is *much weaker* in a similar scan where *temperature gradient and* β' are varied consistently, because the reduced linear drive is off-set by a reduction in β' stabilisation. In a scan where both β and β' are varied consistently (at constant a/L_n, a/L_{T_i}, and a/L_{T_e}), at large β_e (and more importantly large β') hybrid-KBM turbulence is suppressed, leaving a much lower level of turbulent transport driven by subdominant MTMs that are unaffected by β' stabilisation. The residual saturated MTM turbulence drives a modest level of predominantly electron heat transport carried by magnetic flutter.

In addition, microtearing turbulence from the subdominant MTM has been modelled in isolation by artificially (and unphysically) suppressing hybrid-KBMs through the neglect of $\delta B_\parallel$ fluctuations. The MTM-driven heat flux was found to saturate at negligible transport levels on the chosen surface in STEP-EC-HD. Nevertheless, MTM turbulence could be more relevant for transport under different local equilibrium conditions, e.g. when the hybrid-KBM is suppressed.

In conclusion, this study suggests that a transport steady state may exist for a local equilibrium in the vicinity of the $q = 3.5$ surface of the STEP-EC-HD flat-top operating point. It has not, however, yet been assessed whether there is a viable route to access such a burning flat-top on a path that avoids unacceptably large fluxes, e.g. from hybrid-KBM turbulence at lower β'. Nevertheless, the existence of high β local equilibrium regimes with promising transport properties provides a very strong incentive for more detailed future studies over STEP-relevant parameter space, focussing on two main fronts. Firstly, motivated by our results in §2 and §3, we intend to explore higher fidelity GK simulations to assess the validity of the local GK approximation at the onset of large transport fluxes from the hybrid-KBM. In parallel, local gyrokinetics should be used to perform more extensive detailed investigations of regimes where hybrid-KBMs saturate at more modest transport fluxes to better understand the threshold. While the simple scans of §4 provide useful insights, more thorough sensitivity studies are required that ideally also take into account the accessible operation space. A pressing further objective will be to develop a reduced transport model for electromagnetic turbulence that can be used in integrated modelling.

Acknowledgements

The authors would like to thank E. Belli and J. Candy for their very helpful support with CGYRO simulations as well as T. Görler and D. Told for their help with GENE. The authors would also like to thank B. Chapman, D. Hatch, P. Ivanov, and M. Hardman for helpful discussions and suggestions at various stages of this project. D. Kennedy is grateful to The Institute for Fusion Studies (IFS), Austin TX, for its splendid hospitality during a stimulating and productive visit at the beginning of this work. This work has been funded by the Engineering and Physical Sciences Research Council (grant numbers EP/R034737/1 and EP/W006839/1). Simulations have been performed on the ARCHER2 UK National Supercomputing Service under the project e607 and on the Marconi National Supercomputing Consortium CINECA (Italy) under the projects STETGMTM and QLTURB. Part of this work was performed using resources provided by the Cambridge Service for Data Driven Discovery (CSD3) operated by the University of Cambridge Research Computing Service (`www.csd3.cam.ac.uk`), provided by Dell EMC and Intel using Tier-2 funding from the Engineering and Physical Sciences Research Council (capital grant EP/T022159/1), and DiRAC funding from the Science and Technology Facilities Council (`www.dirac.ac.uk`).

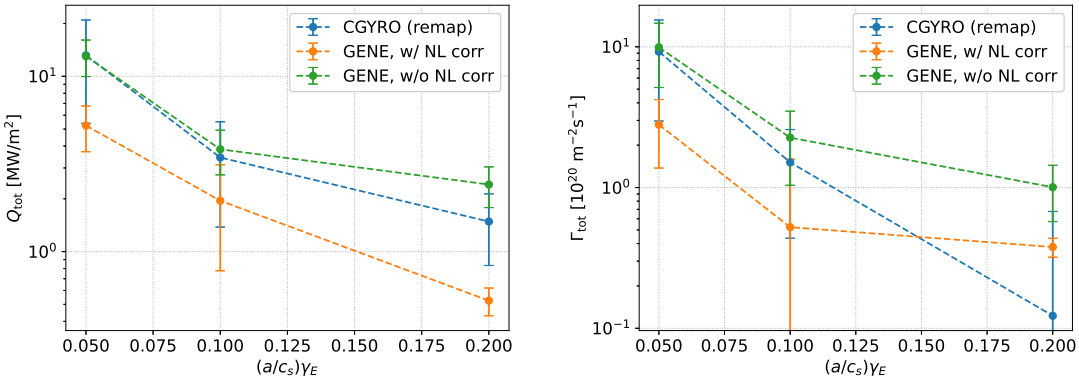

(a) **(b)**

Figure A1: *Total heat (a) and particle (b) flux from CGYRO and GENE nonlinear simulations at different value of external flow shear. Both CGYRO and GENE simulations are performed with the wavenumber remapping implementation of the flow shear. GENE simulations are performed with (orange markers) and without (green markers) the correction to the flow shear implementation of [22].*

Appendix A. Wavenumber remapping implementation of flow shear

The default and recommended treatment of equilibrium flow shear in CGYRO is to use the spectral method, which we have used in the main text. We note, however, that a wavenumber remapping method is also implemented in CGYRO, which is similar to the method used in GENE but excludes the shearing contribution to the nonlinear term [22] (included in GENE). We briefly discuss here the impact of the shearing contribution to the nonlinear term on the saturated heat and particle flux values in STEP simulations. This comparison is shown in Figure A1 at three different values of flow shear. When the nonlinear correction is considered in GENE (the default), the heat flux predicted by GENE is lower than the CGYRO predictions (with the wavenumber implementation of the flow shear) at all the γ_E values considered here. On the other hand, a very good agreement between CGYRO (with the wavenumber implementation of the flow shear) and GENE fluxes is observed in Figure A1 when the nonlinear shearing term is manually removed from the GENE implementation of the flow shear. We note that, in this last case, the wavenumber remapping implementation of the flow shear is identical in CGYRO and GENE.

In this STEP flat-top operating point, the wavenumber remapping implementation overestimates particle and heat fluxes if the nonlinear correction of [22] is removed.

Appendix B. Saturation mechanisms of the MTM instability

Previous theories and simulations of microtearing turbulence have reported various saturation processes through energy transfer to long and short wavelengths [30, 44],

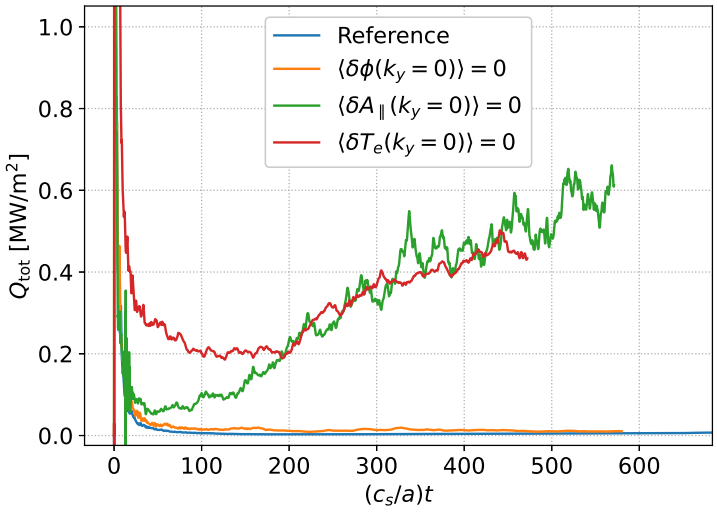

Figure B1: *Time trace of the total heat flux from the nominal GENE simulation (blue line) and three test simulations where the zonal flows (orange line), zonal fields (green line) or zonal temperature (red line) are removed from the system.*

background shear flow [29], zonal fields [33, 34], electron temperature flattening [43], and cross-scale interaction [32]. In the STEP MTM simulations considered here, we find that electron temperature flattening and zonal fields play an important role in the saturation mechanism. As the electrons move swiftly along the perturbed magnetic field lines associated with magnetic islands at the rational surfaces, they undergo a periodic radial excursion, leading to a flattening of the electron temperature. Given that the electron temperature gradient provides the drive for the MTM instability, this flattening can locally stabilise the mode. We test whether this occurs in our simulations by removing the zonal electron temperature perturbations that cause the local temperature flattening, i.e. by redefining the zonal component of the electron distribution function as $\langle\delta f_e^{\rm mod}\rangle_{y,\theta} = \langle\delta f_e\rangle_{y,\theta} - K(r)[m_e v^2/(2T_e) - 1.5]\langle F_{e0}\rangle_{y,\theta}$, where $\langle\cdot\rangle_{y,\theta}$ denotes the flux-surface average, F_{e0} is the electron background Maxwellian distribution function and $K(r)$ is a function of the radial coordinate only, which is set at each time step such that $\langle\delta T_e\rangle_{y,\theta} = 0$ [43]. The resulting simulation, shown in Figure B1, returns a much larger heat flux than the reference case. Zonal fields can also provide a strong saturation mechanism for MTM turbulence by reducing the amplitude of non-zonal $\delta A_\parallel$ modes and the subsequent magnetic stochasticity. We also perform a nonlinear test simulation where the zonal fields are removed. As shown in Figure B1, this test simulation also returns much larger heat flux than the nominal simulation. Interestingly, the time trace of the heat flux from the two test simulations agrees very well, thus suggesting a competition (or a link) between zonal fields and local temperature flattening as saturation mechanisms. An additional simulation test also in Fig. B1 shows that zonal flows are not relevant for MTM turbulence saturation, at least in the case considered here.

References

[1] D. Kennedy, M. Giacomin, F. Casson, D. Dickinson, W. A. Hornsby, B. S. Patel, and C. M. Roach. Electromagnetic gyrokinetic instabilities in the Spherical Tokamak for Energy Production (STEP) part I: linear physics and sensitivity. *submitted to Nuclear Fusion*, 2023.

[2] B. Patel. *Confinement physics for a steady state net electric burning spherical tokamak*. PhD thesis, University of York, 2021.

[3] D. Dickinson, M. S. Anastopoulos-Tzanis, A. Bokshi, R. Davies, M. Giacomin, D. Kennedy, B. S. Patel, L. Richardson, C. M. Roach, and H. R. Wilson. Microstability and transport in high-β spherical tokamaks. 2023. Zenodo, `https://doi.org/10.5281/zenodo.7961621`.

[4] W. J Nuttall, S. Konishi, S. Takeda, and D. Webbe-Wood, editors. *in Commercialising Fusion Energy*. 2053-2563. IOP Publishing, 2020.

[5] STEP - Spherical Tokamak for Energy Production. `https://step.ukaea.uk/`.

[6] S M Kaye, J W Connor, and C M Roach. Thermal confinement and transport in spherical tokamaks: a review. *Plasma Physics and Controlled Fusion*, 63(12):123001, 2021.

[7] M. J. Pueschel, D. R. Hatch, T. Görler, W. M. Nevins, F. Jenko, P. W. Terry, and D. Told. Properties of high-β microturbulence and the non-zonal transition. *Physics of Plasmas*, 20(10):102301, 2013.

[8] M. Romanelli, G. Corrigan, V. Parail, S. Wiesen, R. Ambrosino, et al. Jintrac: A system of codes for integrated simulation of tokamak scenarios. *Plasma and Fusion Research*, 9:3403023–3403023, 2014.

[9] M. Erba, A. Cherubini, V. V. Parail, E. Springmann, and A. Taroni. Development of a non-local model for tokamak heat transport in l-mode, h-mode and transient regimes. *Plasma Physics and Controlled Fusion*, 39(2):261, 1997.

[10] H Meyer for the STEP Plasma Control, Heating, Current Drive Team, and Contributors. The physics of the preferred plasma scenario for step. In *Proceedings of the 48th EPS Conference on Plasma Physics*, June 2022.

[11] Tholerus. E. The operational space of step powerplant operating power point. unpublished, in-perparation, N.D.

[12] R. L. Miller, M. S. Chu, J. M. Greene, Y. R. Lin-Liu, and R. E. Waltz. Noncircular, finite aspect ratio, local equilibrium model. *Physics of Plasmas*, 5(4):973–978, 1998.

[13] B.S. Patel, L. Pattinson, P. Hill, M. Giacomin, D. Kennedy, D. Dickinson, H.G. Dudding, F.J. Casson, and A.C. Jayalekshmi. pyrokinetics, 10 2022.

[14] J. Candy, E. A. Belli, and R. V. Bravenec. A high-accuracy Eulerian gyrokinetic solver for collisional plasmas. *Journal of Computational Physics*, 324:73–93, 2016.

[15] F. Jenko, W. Dorland, M. Kotschenreuther, and B. N. Rogers. Electron temperature gradient driven turbulence. *Physics of Plasmas*, 7(5):1904–1910, 2000.

[16] M. Barnes, D. Dickinson, W. Dorland, P. A. Hill, C. M. Parker, J. T.and Roach, S. Biggs-Fox, N. Christen, R. Numata, et al. GS2 v8.1.2, 10.5281/zenodo.6882296, 2022.

[17] H Sugama, T-H Watanabe, and M Nunami. Linearized model collision operators for multiple ion species plasmas and gyrokinetic entropy balance equations. *Physics of Plasmas*, 16(11):112503, 2009.

[18] M. Barnes, I. G. Abel, W. Dorland, D. R. Ernst, G. W. Hammett, P. Ricci, B. N. Rogers, A. A. Schekochihin, and T. Tatsuno. Linearized model Fokker–Planck collision operators for gyrokinetic simulations. II. Numerical implementation and tests. *Physics of Plasmas*, 16(7):072107, 2009.

[19] J. F. Parisi, F. I. Parra, C. M. Roach, C. Giroud, W. Dorland, D. R. Hatch, M. Barnes, J. C. Hillesheim, N. Aiba, J. Ball, et al. Toroidal and slab etg instability dominance in the linear spectrum of jet-ilw pedestals. *Nuclear Fusion*, 60(12):126045, 2020.

[20] J. Candy and E. A. Belli. Spectral treatment of gyrokinetic shear flow. *Journal of Computational Physics*, 356:448–457, 2018.

[21] GW Hammett, W Dorland, NF Loureiro, and T Tatsuno. Implementation of large scale E× B shear flow in the GS2 gyrokinetic turbulence code. In *48th Annual Meeting of the Division of Plasma Physics*, 2006.

[22] B. F. McMillan, J. Ball, and S. Brunner. Simulating background shear flow in local gyrokinetic simulations. *Plasma Physics and Controlled Fusion*, 61(5):055006, 2019.

[23] F. Van Wyk, E. G. Highcock, A. R. Field, C. M. Roach, A. A. Schekochihin, F. I. Parra, and W. Dorland. Ion-scale turbulence in mast: anomalous transport, subcritical transitions, and comparison to bes measurements. *Plasma Physics and Controlled Fusion*, 59(11):114003, 2017.

[24] N. Christen, M. Barnes, and F. I. Parra. Continuous-in-time approach to flow shear in a linearly implicit local gyrokinetic code. *Journal of Plasma Physics*, 87(2):905870230, 2021.

[25] C M Roach, J W Connor, and S Janjua. Trapped particle precession in advanced tokamaks. *Plasma Physics and Controlled Fusion*, 37(6):679, 1995.

[26] C. Bourdelle, G.T. Hoang, X. Litaudon, C.M. Roach, and T. Tala. Impact of the α parameter on the microstability of internal transport barriers. *Nuclear Fusion*, 45(2):110, 2005.

[27] H.R. Wilson, J.-W. Ahn, R.J. Akers, D. Applegate, R.A. Cairns, J.P. Christiansen, J.W. Connor, G. Counsell, A. Dnestrovskij, W.D. Dorland, M.J. Hole, N. Joiner, A. Kirk, P.J. Knight, C.N. Lashmore-Davies, K.G. McClements, D.E. McGregor, M.R. O'Brien, C.M. Roach, S. Tsaun, and G.M. Voss. Integrated plasma physics modelling for the culham steady state spherical tokamak fusion power plant. *Nuclear Fusion*, 44(8):917, 2004.

[28] B. S. Patel, D. Dickinson, C. M. Roach, and H. Wilson. Linear gyrokinetic stability of a high β non-inductive spherical tokamak. *Nuclear Fusion*, 62(1):016009, 2021.

[29] W. Guttenfelder, J. Candy, S. M. Kaye, W. M. Nevins, E. Wang, R. E. Bell, G. W. Hammett, B. P. LeBlanc, D. R. Mikkelsen, and H. Yuh. Electromagnetic transport from microtearing mode turbulence. *Physical Review Letters*, 106(15):155004, 2011.

[30] H. Doerk, F. Jenko, M. J. Pueschel, and D. R. Hatch. Gyrokinetic microtearing turbulence. *Physical Review Letters*, 106(15):155003, 2011.

[31] D. R. Hatch, M. Kotschenreuther, S. Mahajan, P. Valanju, F. Jenko, D. Told, T. Görler, and S. Saarelma. Microtearing turbulence limiting the JET-ILW pedestal. *Nuclear Fusion*, 56(10):104003, 2016.

[32] S. Maeyama, T-H Watanabe, and A. Ishizawa. Suppression of ion-scale microtearing modes by electron-scale turbulence via cross-scale nonlinear interactions in tokamak plasmas. *Physical Review Letters*, 119(19):195002, 2017.

[33] M. J. Pueschel, D. R. Hatch, M. Kotschenreuther, A. Ishizawa, and G. Merlo. Multi-scale interactions of microtearing turbulence in the tokamak pedestal. *Nuclear Fusion*, 60(12):124005, 2020.

[34] M. Giacomin, D. Dickinson, D. Kennedy, B. Patel, and C.M. Roach. Investigations of stochastic layer formation in first nonlinear microtearing mode simulations for MAST. *arXiv:2303.02379*, 2023.

[35] M. T. Curie, J. L. Larakers, D. R. Hatch, A. O. Nelson, A. Diallo, E. Hassan, W. Guttenfelder, M. Halfmoon, M. Kotschenreuther, R. D. Hazeltine, S. M. Mahajan, R. J. Groebner, J. Chen, C. Perez von Thun, L. Frassinetti, S. Saarelma, C. Giroud, and M. M. Tennery. A survey of pedestal magnetic fluctuations using gyrokinetics and a global reduced model for microtearing stability. *Physics of Plasmas*, 29(4):042503, 2022.

[36] M. Kotschenreuther, X. Liu, D. Hatch, S. Mahajan, L. Zheng, A. Diallo, R. Groebner, J. Hillesheim, C. Maggi, C. Giroud, F. Koechl, V. Parail, S. Saarelma, E. Solano, and A. Chankin. Gyrokinetic analysis and simulation of pedestals to identify the culprits for energy losses using 'fingerprints. *Nucl. Fusion*, 59:096001, 2019.

[37] J. Chen, D. L. Brower, W. X. Ding, Z. Yan, T. Osborne, E. Strait, M. Curie, D. R. Hatch, M. Kotschenreuther, X. Jian, M. R. Halfmoon, and S. M. Mahajan. Internal measurement of magnetic turbulence in elmy h-mode tokamak plasmas. *Phys. Plasmas*, 27:120701, 2020.

[38] D. Hatch, M. Kotschenreuther, S. Mahajan, M. Pueschel, C. Michoski, G. Merlo, E. Hassan,

A. Field, L. Frassinetti, C. Giroud, J. Hillesheim, C. Maggi, C. P. von Thun, C. Roach, S. Saarelma, D. Jarema, and F. Jenko. Microtearing modes as the source of magnetic fluctuations in the JET pedestal. *Nucl. Fusion*, 61:036015, 2021.

[39] E. Hassan, D. Hatch, M. Halfmoon, M. Curie, M. Kotchenreuther, S. Mahajan, G. Merlo, R. Groebner, A. Nelson, and A. Diallo. Identifying the microtearing modes in the pedestal of diii-d h-modes using gyrokinetic simulations. *Nucl. Fusion*, 62:026008, 2021.

[40] A. O. Nelson, F. M. Laggner, A. Diallo, D. Smith, A. Xing, R. Shousha, and E. Kolemen. Time-dependent experimental identification of inter-elm microtearing modes in the tokamak edge on diii-d. *Nucl. Fusion*, 61:116038, 2021.

[41] A. Diallo, J. Dominski, K. Barada, M. Knolker, G. J. Kramer, and G. McKee. Direct observation of nonlinear coupling between pedestal modes leading to the onset of edge localized modes. *Phys. Rev. Lett.*, 121:235001, 2018.

[42] D. J. Applegate, CM Roach, J. W. Connor, S. C. Cowley, W. Dorland, R. J. Hastie, and N. Joiner. Micro-tearing modes in the mega ampere spherical tokamak. *Plasma Physics and Controlled Fusion*, 49(8):1113, 2007.

[43] Ajay C.J., B.F. McMillan, and M.J. Pueschel. On the impact of temperature gradient flattening and system size on heat transport in microtearing turbulence. *Nuclear Fusion*, 63(6):066024, 2023.

[44] J. F. Drake, N. T. Gladd, C. S. Liu, and C. L. Chang. Microtearing modes and anomalous transport in tokamaks. *Physical Review Letters*, 44(15):994, 1980.